Binuclear Oxidative Additions of Silanes to $[Ir_2(CO)_3(Ph_2PCH_2PPh_2)_2]$ To Yield Silylene-Bridged Dihydride Complexes

Robert McDonald and Martin Cowie*

Department of Chemistry, The University of Alberta, Edmonton, Alberta, Canada T6G 2G2

Received December 15, 1989

The complex $[Ir_2(CO)_3(dppm)_2]$ (1; dppm = $Ph_2PCH_2PPh_2$) reacts with the secondary silanes Me_2SiH_2, Et_2SiH_2, and Ph_2SiH_2 to give products of the form $[Ir_2(H)_2(CO)_2(\mu\text{-}SiR_2)(dppm)_2]$ (R = Me (2), Et (3), Ph (4)). These silylene-bridged species are found to be fluxional at room temperature. Reaction of 1 with $PhSiH_3$ yields $[Ir_2(H)_2(CO)_2(\mu\text{-}SiHPh)(dppm)_2]$ (5), which is not fluxional. The X-ray structures of 4 and 5 have been determined and show that both species have bridging silylene groups, terminal hydride ligands, and cis arrangements of the phosphine ligands about each metal center. Compound 4 displays a twisted configuration showing substantial steric interaction between the μ-diphenylsilylene group and the dppm phenyls, suggesting the genesis for fluxionality of this species. In contrast, species 5 appears to be relatively free of such steric encumbrance, with the phenyl group of the bridging phenylsilylene unit held away from the dppm phenyl groups. In this complex the dppm ligands are disposed in an eclipsed manner about the two metals. The similarities of the low-temperature ^1H and $^{31}P\{^1H\}$ NMR spectra of 2 and 3 to those of 5 at room temperature indicate that a structure similar to that of 5 may be the low-temperature configuration adopted by the dialkylsilylene-bridged dimers. Complex 4 crystallizes with two THF solvent molecules in the trigonal space group $P3_121$ with a = 13.295 (3) Å, c = 32.286 (4) Å, and Z = 3. This structure was refined to R = 0.038 and R_w = 0.039 on the basis of 3288 unique observed reflections and 229 parameters varied. Complex 5 crystallizes with two THF solvent molecules in the monoclinic space group $P2_1/c$ with a = 12.425 (3) Å, b = 20.282 (4) Å, c = 26.505 (3) Å, β = 97.61 (1)°, and Z = 4. This structure was refined to R = 0.061 and R_w = 0.087 on the basis of 4697 unique observed reflections and 334 parameters varied.

Introduction

The formation of transition-metal-to-silicon bonds is a fundamental step in several metal-catalyzed processes, including olefin hydrosilylation,[1] silane alcoholysis,[2] and the oligomerization of silanes.[3] Among the many approaches taken to promote Si–M bond formation,[4] the oxidative addition of Si–H bonds to low-valent metal centers is of interest to this research group in that it may offer insights into C–H bond activation processes[5] promoted by adjacent metals, as well as into the activation of other heteroatom–hydrogen bonds by multicenter complexes. As part of an ongoing study of possible cooperative effects between adjacent metal nuclei in the activation of H–H and heteroatom–hydrogen bonds,[6-9] we have been investigating the reactions of silanes with the low-valent complexes $[MM'(CO)_3(dppm)_2]$ (M = M' = Ir; M = Rh, M' = Ir); closely related studies involving the dirhodium analogue $[Rh_2(CO)_3(dppm)_2]$ have recently been reported by Eisenberg and co-workers.[10] Although the metals in these complexes are formally zerovalent, recent work[7] suggests that these complexes are more appropriately formulated as mixed-valence species, in which the metals are involved in a dative M(−1)–M(+1) bond. Whatever the oxidation-state formulation for these complexes, the metals are certainly of low valence and thus should be susceptible to oxidation; in addition, the coordinative unsaturation at one of the metal centers offers the possibility of initial substrate coordination as a prelude to oxidative addition to the complex. In an effort to utilize both metals in substrate activation, we have been investigating the reactivities of H_2X-type molecules (X = S, Se, SiR_2, SiHR), in which both geminal X–H bonds are potentially reactive. We are particularly interested in establishing how such substrates interact with the two metal nuclei during the proposed "double-activation" process. Herein we report the results of our studies on the reactions between $[Ir_2(CO)_3(dppm)_2]$ and some primary and secondary alkyl- and arylsilanes.

Experimental Section

All solvents were dried and distilled before use and were stored under N_2. Reactions were carried out at room temperature by using standard Schlenk procedures unless otherwise noted. Dinitrogen was passed through columns of Ridox and 4A molecular sieves to remove traces of oxygen and water, respectively. Hydrated iridium(III) chloride was purchased from Engelhard Scientific, bis(diphenylphosphino)methane (dppm) was purchased from Organometallics Inc., and silane reagents were purchased from Petrarch Systems Inc. The complex $[Ir_2(CO)_3(dppm)_2]$ (1) was prepared as previously reported.[6] All other chemicals were used as received without further purification.

NMR spectra were recorded on a Bruker AM-400 spectrometer operating at 400 MHz for ^1H and $^1H\{^{31}P\}$ spectra, at 161.9 MHz for $^{31}P\{^1H\}$ spectra, and at 100.6 MHz for $^{13}C\{^1H\}$ spectra.

(1) Speier, J. L. *Adv. Organomet. Chem.* **1979**, *17*, 407.
(2) (a) Ojima, I.; Kogure, T.; Nihonyanagi, M.; Kono, H.; Inaba, S.; Nagai, Y. *Chem. Lett.* **1973**, 501. (b) Corriu, R. J. P.; Moreau, J. J. E. *J. Organomet. Chem.* **1976**, *114*, 135. (c) Blackburn, S. N.; Haszeldine, R. N.; Parish, R. V.; Setchfi, J. H. *J. Organomet. Chem.* **1980**, *192*, 329. (d) Dwyer, J.; Hilal, H. S.; Parish, R. V. *J. Organomet. Chem.* **1982**, *228*, 191. (e) Lukevics, E.; Dzintara, M. *J. Organomet. Chem.* **1985**, *295*, 265.
(3) (a) Yamamoto, K.; Okinoshima, H.; Kumada, M. *J. Organomet. Chem.* **1971**, *27*, C31. (b) Ojima, I.; Inaba, S.-I.; Kogure, T.; Nagai, Y. *J. Organomet. Chem.* **1973**, *55*, C7. (c) Lappert, M. F.; Maskell, R. K. *J. Organomet. Chem.* **1984**, *264*, 217. (d) Brown-Wensley, K. A. *Organometallics* **1987**, *6*, 1590. (e) Corey, J. Y.; Chang, L. S.; Corey, E. R. *Organometallics* **1987**, *6*, 1595.
(4) Mackay, K. M.; Nicholson, B. K. In *Comprehensive Organometallic Chemistry*; Wilkinson, G., Stone, F. G. A., Abel, E. W., Eds.; Pergamon Press: Oxford, England, 1982; Chapter 43.
(5) Graham, W. A. G. *J. Organomet. Chem.* **1986**, *300*, 81.
(6) Sutherland, B. R.; Cowie, M. *Organometallics* **1985**, *4*, 1637.
(7) McDonald, R.; Cowie, M. *Inorg. Chem.* **1990**, *29*, 1564.
(8) Antonelli, D. M.; Cowie, M. *Inorg. Chem.*, in press.
(9) Vaartstra, B. A.; Cowie, M. *Inorg. Chem.* **1989**, *28*, 3138.
(10) (a) Wang, W.-D.; Hommeltoft, S. I.; Eisenberg, R. *Organometallics* **1988**, *7*, 2417. (b) Wang, W.-D.; Eisenberg, R. *J. Am. Chem. Soc.* **1990**, *112*, 1833.

0276-7333/90/2309-2468$02.50/0

Table I. Spectroscopic Data[a]

compd	IR, cm^{-1} solid[b]	IR, cm^{-1} soln[c]	NMR $\delta(^{31}P\{^1H\})$[d]	NMR $\delta(^1H)$[e]
$[Ir_2(H)_2(CO)_2(\mu\text{-}SiMe_2)(dppm)_2]$ (2)	1944 (st),[f] 1935 (vs),[f] 2012 (w)[g]	1945 (sh),[f] 1930 (vs, br),[f] 2010 (w)[g]	−13.3 (s, br)	7.38–6.86 (mult, 40 H), 6.18 (mult, 2 H), 2.98 (mult, 2 H), 0.70 (s, br, 6 H), −11.49 (mult, 2 H)
$[Ir_2(H)_2(CO)_2(\mu\text{-}SiEt_2)(dppm)_2]$ (3)	1942 (st),[f] 1929 (vs),[f] 2007 (w)[g]	1940 (sh),[f] 1926 (vs, br),[f] 2015 (w)[g]	−14.5 (s, br)	7.65–6.83 (mult, 40 H), 6.17 (mult, 2 H), 2.99 (mult, 2 H), 1.13 (t, $^3J_{H-H}$ = 7.6 Hz, 6 H), 0.88 (q, $^3J_{H-H}$ = 7.6 Hz, 4 H), −11.69 (mult, 2 H)
$[Ir_2(H)_2(CO)_2(\mu\text{-}SiPh_2)(dppm)_2]$ (4)	1929 (vs),[f] 2098 (w)[g]	1933 (vs, br),[f] 2096 (w)[g]	−17.3 (s, br)	7.69–6.73 (mult, 50 H), 5.76 (br, 2 H), 3.29 (mult, 2 H), −11.99 (mult, 2 H)
$[Ir_2(H)_2(CO)_2(\mu\text{-}SiHPh)(dppm)_2]$ (5)	1942 (vs),[f] 2061 (w),[h] 2108 (w)[g]	1940 (vs, br),[f] 2070 (w),[h] 2108 (w)[g]	−8.4 (s, br), −19.1 (s, br)	8.19–6.79 (mult, 45 H), 6.72 (s, 1 H), 6.39 (mult, 1 H), 6.08 (mult, 1 H), 3.22 (mult, 1 H), 2.82 (mult, 1 H), −11.43 (mult, 2 H)

[a] Abbreviations used: w = weak, m = medium, st = strong, vs = very strong, sh = shoulder, br = broad, s = singlet, t = triplet, q = quartet, mult = multiplet. [b] Nujol mull on KBr disk. [c] CH_2Cl_2 solution in KCl cells. [d] Vs 85% H_3PO_4, 25 °C, in CD_2Cl_2 solvent. [e] Vs TMS, 25 °C, in CD_2Cl_2 solvent. [f] ν(CO). [g] ν(IrH). [h] ν(SiH).

Phosphorus chemical shifts are reported with respect to external 85% H_3PO_4, while carbon and proton shifts are with respect to TMS with the solvent as internal standard. Infrared spectra were run on either a Nicolet 7199 Fourier transform interferometer or a Perkin-Elmer 883 spectrophotometer, as either solids (Nujol mulls on KBr disks) or solutions (KCl cell windows, 0.5-mm path length). Spectroscopic parameters for the compounds prepared are found in Table I. Elemental analyses were performed by the microanalytical service within the department.

Preparation of Compounds. (a) $[Ir_2(H)_2(CO)_2(\mu\text{-}SiMe_2)(dppm)_2]$ (2). Dimethylsilane was slowly bubbled (~0.25 mL/s) through a solution of **1** (150 mg, 121 μmol) in THF (10 mL) for ca. 30 s, producing an immediate color change from orange to light yellow. The reaction mixture was stirred for 10 min and the solution volume then reduced under an N_2 stream to 2 mL; addition of hexane (20 mL) caused precipitation of a golden yellow solid. Recrystallization from THF/ether afforded **2** as a bright yellow powder (131 mg, 86% isolated yield). Anal. Calcd for $C_{54}H_{52}Ir_2O_2P_4Si$: C, 51.09; H, 4.13. Found: C, 50.93; H, 4.13.

(b) $[Ir_2(H)_2(CO)_2(\mu\text{-}SiEt_2)(dppm)_2]$ (3). Diethylsilane (15.6 μL, 10.7 mg, 121 μmol) was added to a solution of **1** (150 mg, 121 μmol) in THF (10 mL). Within 30 min the solution color had changed from orange to light yellow. Reduction of solution volume to 2 mL followed by addition of hexane (20 mL) produced a golden yellow solid. Complex **3** was recrystallized from THF/ether to give 121 mg (77%) of yellow powder. Anal. Calcd for $C_{56}H_{56}Ir_2O_2P_4Si$: C, 51.84; H, 4.35. Found: C, 51.38, H, 4.10.

(c) $[Ir_2(H)_2(CO)_2(\mu\text{-}SiPh_2)(dppm)_2]$ (4). To a solution of **1** (150 mg, 121 μmol) in THF (10 mL) was added diphenylsilane (22.4 μL, 22.3 mg, 121 μmol). After 2 h the solution color had changed from orange to light yellow, accompanied by formation of yellow solid. Precipitation was completed via addition of hexane (20 mL). The product was recrystallized from THF/ether and then dried in vacuo, affording **4** as a light yellow solid (139 mg, 82%). Anal. Calcd for $C_{64}H_{56}Ir_2O_2P_4Si$: C, 55.16; H, 4.05. Found: C, 55.37; H, 4.47.

(d) $[Ir_2(H)_2(CO)_2(\mu\text{-}SiHPh)(dppm)_2]$ (5). Addition of phenylsilane (20.2 μL, 17.5 mg, 162 μmol) to a solution of **1** (200 mg, 162 μmol) in THF (5 mL) produced an immediate change in color from orange to yellow; within 1 h a yellow precipitate formed. Diethyl ether (20 mL) was added to complete precipitation, and recrystallizing from THF/ether and drying under vacuum resulted in the isolation of **5** as a pale yellow solid (178 mg, 84%). Anal. Calcd for $C_{58}H_{52}Ir_2O_2P_4Si$: C, 52.88; H, 3.98. Found: C, 53.12; H, 4.53.

Reaction of 1 with Me_3SiH. Trimethylsilane was slowly bubbled (~0.25 mL/s) through a rapidly stirred solution of **1** (65 mg, 52.5 μmol) in THF (3 mL) for 1 min. After 10 min the solution color had changed from orange to light yellow. The product was found by ^1H and $^{31}P\{^1H\}$ NMR spectroscopy to be the previously characterized $[Ir_2(H)_4(CO)_2(dppm)_2]$.[11]

(11) McDonald, R.; Sutherland, B. R.; Cowie, M. *Inorg. Chem.* **1987**, *26*, 3333.

Table II. Crystallographic Data for $[Ir_2(H)_2(CO)_2(\mu\text{-}SiPh_2)(dppm)_2]\cdot 2THF$ (4) and $[Ir_2(H)_2(CO)_2(\mu\text{-}SiHPh)(dppm)_2]\cdot 2THF$ (5)

compd	4	5
formula	$C_{72}H_{72}Ir_2O_4P_4Si$	$C_{66}H_{68}Ir_2O_4P_4Si$
fw	1537.80	1461.70
space group	$P3_121$ (No. 152)	$P2_1/c$ (No. 14)
temp, °C	22	
radiation (λ, Å)	graphite-monochromated Mo Kα (0.710 69)	
unit cell params		
a, Å	13.295 (3)	12.425 (3)
b, Å		20.282 (4)
c, Å	32.286 (4)	26.505 (3)
β, deg		97.61 (1)
V, Å^3	4941 (2)	6621 (3)
Z	3	4
ρ(calcd), g cm^{-3}	1.550	1.466
linear abs coeff (μ), cm^{-1}	41.799	41.550
range of transmissn factors	0.852–1.095	0.660–1.286
R^a	0.038	0.061
$R_w{}^b$	0.039	0.087

[a] $R = \sum||F_o| - |F_c||/\sum|F_o|$. [b] $R_w = [\sum w(|F_o| - |F_c|)^2/\sum wF_o^2]^{1/2}$, where $w = 4F_o^2/\sigma^2(F_o^2)$.

Reaction of $[Ir_2(CO)_2(\mu\text{-}H)_2(dppm)_2]$ with Me_3SiH. A solution of $[Ir_2(CO)_2(\mu\text{-}H)_2(dppm)_2]$ was generated by reaction of $[Ir_2(H)(CO)_2(\mu\text{-}H)_2(dppm)_2][BF_4]$ (70 mg, 53.9 μmol) with potassium *tert*-butoxide (6.0 mg, 53.9 μmol) in THF (2 mL) at 0 °C.[11] Trimethylsilane was slowly bubbled (~0.25 mL/s) through this solution for 1 min, during which time the color changed from deep red to medium yellow. The product was found by IR and $^{31}P\{^1H\}$ NMR spectroscopy to be $[Ir_2(H)_4(CO)_2(dppm)_2]$.[11]

X-ray Data Collection. (a) $[Ir_2(H)_2(CO)_2(\mu\text{-}SiPh_2)(dppm)_2]\cdot 2THF$ (4). Colorless crystals of **4** were grown through diffusion of ether into a concentrated THF solution of the complex. Suitable crystals were mounted and flame-sealed in glass capillaries under N_2 and solvent vapor to minimize decomposition and/or solvent loss. Data were collected on an Enraf-Nonius CAD4 diffractometer using Mo Kα radiation. Unit-cell parameters were obtained from a least-squares refinement of the setting angles of 25 reflections in the range $20.0° \le 2\theta \le 24.0°$. The systematic absences ($00l$, $l \neq 3n$) and the $\bar{3}m1$ diffraction symmetry suggested one of the trigonal space groups $P3_121$ and $P3_221$. The space group $P3_121$ was confirmed by the successful solution and refinement of the structure. Refinement of the structure in the enantiomeric space group $P3_221$ gave significantly poorer residuals (R = 0.056 and R_w = 0.067 for the trial space group vs R = 0.038 and R_w = 0.040 for the correct space group at the same stage of refinement).

Intensity data were collected at 22 °C by using the ω-scan technique to a maximum $2\theta = 50.0°$, covering the quadrant $\pm h, +k, +l$. Of the data collected, 5803 reflections were unique after merging. Backgrounds were scanned for 25% of the peak width on either side of the peak scan. Three reflections were chosen as intensity standards, being remeasured after every 120

min of X-ray exposure time. Each standard lost approximately 15% of its original intensity; thus, a linear decomposition correction was applied to the data. The data were measured and processed in the usual way, with a value of 0.04 for p[12] employed to downweight intense reflections; 3288 reflections were considered observed and were used in subsequent calculations. Absorption corrections were applied to the data according to Walker and Stuart's method.[13,14]

(b) $[Ir_2(H)_2(CO)_2(\mu\text{-SiHPh})(dppm)_2]\cdot 2THF$ (5). Pale yellow crystals of **5** were obtained by diffusion of hexane into a THF solution of the complex. Crystals were mounted in glass capillaries under N_2 and solvent vapor. Data collection and derivation of unit-cell parameters proceeded in a manner similar to that above. The monoclinic diffraction symmetry and systematic absences ($h0l$, l = odd; $0k0$, k = odd) were consistent with the space group $P2_1/c$.

Intensity data were collected at 22 °C with use of the $\theta/2\theta$ scan technique to a maximum $2\theta = 50.0°$. The intensity standards were found to lose 20–30% of their initial intensity, necessitating application of a linear decomposition correction. Of 11 952 unique reflections measured, 4697 were considered observed for the purposes of subsequent calculations, with absorption corrections applied as above.

Structure Solution and Refinement. Both structures were solved in the respective space groups ($P3_121$ for **4**, $P2_1/c$ for **5**) with use of standard Patterson and Fourier techniques. Full-matrix least-squares refinements proceeded so as to minimize the function $\sum w(|F_o| - |F_c|)^2$, where $w = 4F_o^2/\sigma^2(F_o^2)$. Atomic scattering factors and anomalous dispersion terms were taken from the usual tabulations.[15-17] Positional parameters for the hydrogens attached to the carbon atoms of the complexes (as well as to the carbons of the solvent molecules in the structure of **4** and to the silicon atom of **5**) were calculated from the geometries about the attached carbon (or silicon). These hydrogens were located 0.95 Å from their attached C atoms (1.35 Å in the case of Si–H), given thermal parameters 20% greater than the equivalent isotropic B's of their attached atoms, and included as fixed contributions.

In addition to all non-hydrogen atoms of the complex and its solvent molecules, the hydrogen atoms attached to the Ir centers of **4** were also located and refined. Only the non-hydrogen atoms of complex **5** were refined; the electron density due to the solvent molecules was found to be smeared in such a way as to indicate severe rotational disorder of these groups, and attempts to assign and refine carbon or oxygen atoms were unsuccessful. Instead, all solvent atoms were input as carbon atoms in five-membered rings that most appropriately described the electron density. These atoms were assigned large thermal parameters and were not refined in subsequent least-squares cycles. For this reason the solvent molecules' hydrogen atoms were not included. A difference Fourier map calculated with use of all data displayed peaks in the expected positions of the hydride ligands. However, when only low-angle data ($(\sin\theta)/\lambda \leq 0.25$) were used in the Fourier synthesis, the peak corresponding to H(2) could no longer be unambiguously identified, although that due to H(1) was observed in its original location. Owing to the uncertainty in the identification of H(2), neither atom was refined; instead, both were included as fixed contributions in the structure factor calculations, in their positions obtained from the full-data Fourier map. Other hydrogens were included in their idealized positions and handled as described for compound **4**.

The final model for complex **4**, with 229 parameters varied, converged to values of $R = 0.038$ and $R_w = 0.039$. In the final difference Fourier map the 10 highest residuals (0.8–0.7 e/Å^3) were found in the vicinity of the dppm ligands (a typical carbon in an earlier synthesis had an electron density of 3.4 e/Å^3). For compound **5** the final model, with 334 parameters varied, converged to values of $R = 0.061$ and $R_w = 0.087$. The 10 highest residuals in the final difference Fourier map (1.5–0.9 e/Å^3) were found in the area of the solvent molecules (a typical carbon in an earlier synthesis had an electron density of 2.9 e/Å^3). The badly disordered solvent molecules prevented more satisfactory refinement of the structure; however, the parameters within the complex molecule should not be significantly affected. The positional and thermal parameters for the non-hydrogen atoms of complex **4** are given in Table III, and selected bond lengths and angles are given in Tables IV and V, respectively. For complex **5** the pertinent data are found in Tables VI–VIII. Additional information is

Table III. Positional and Thermal Parameters of the Atoms of $[Ir_2(H)_2(CO)_2(\mu\text{-SiPh}_2)(dppm)_2]\cdot 2THF$ (4)[a]

atom	x	y	z	B, Å^2
Ir	0.27192 (3)	0.09855 (3)	−0.14031 (1)	3.211 (8)
P(1)	0.3883 (2)	0.0423 (2)	−0.10409 (9)	3.61 (7)
P(2)	0.1982 (2)	−0.1937 (2)	−0.13619 (9)	3.78 (7)
Si	0.0797 (3)	0.000	−0.167	3.9 (1)
O(1)	0.2681 (8)	0.2940 (7)	−0.0960 (3)	9.0 (3)
C(1)	0.272 (1)	0.2221 (9)	−0.1141 (4)	6.0 (4)
C(2)	0.3436 (8)	−0.1096 (9)	−0.1152 (3)	4.2 (3)
C(11)	0.3738 (8)	0.0425 (8)	−0.0466 (3)	4.4 (3)[b]
C(12)	0.3034 (9)	0.0777 (9)	−0.0290 (4)	5.6 (3)[b]
C(13)	0.295 (1)	0.078 (1)	0.0151 (4)	6.6 (3)[b]
C(14)	0.361 (1)	0.048 (1)	0.0380 (4)	7.1 (4)[b]
C(15)	0.435 (1)	0.016 (1)	0.0220 (4)	7.2 (4)[b]
C(16)	0.4416 (9)	0.0161 (9)	−0.0221 (4)	5.5 (3)[b]
C(21)	0.5477 (8)	0.1149 (8)	−0.1093 (3)	4.6 (3)[b]
C(22)	0.6044 (9)	0.2347 (9)	−0.1055 (4)	5.9 (3)[b]
C(23)	0.730 (1)	0.300 (1)	−0.1076 (4)	7.3 (4)[b]
C(24)	0.786 (1)	0.237 (1)	−0.1128 (5)	8.5 (4)[b]
C(25)	0.731 (1)	0.120 (1)	−0.1161 (5)	8.3 (4)[b]
C(26)	0.610 (1)	0.058 (1)	−0.1153 (4)	6.1 (3)[b]
C(31)	0.0999 (9)	−0.2315 (9)	−0.0920 (3)	4.4 (2)[b]
C(32)	0.136 (1)	−0.226 (1)	−0.0516 (4)	6.3 (3)[b]
C(33)	0.048 (1)	−0.268 (1)	−0.0195 (4)	7.1 (4)[b]
C(34)	−0.063 (1)	−0.315 (1)	−0.0286 (4)	7.8 (4)[b]
C(35)	−0.102 (1)	−0.328 (1)	−0.0686 (4)	8.7 (4)[b]
C(36)	−0.015 (1)	−0.282 (1)	−0.1009 (4)	6.0 (3)[b]
C(41)	0.1825 (8)	−0.3374 (9)	−0.1457 (3)	4.0 (2)[b]
C(42)	0.092 (1)	−0.415 (1)	−0.1691 (4)	7.9 (4)[b]
C(43)	0.078 (1)	−0.527 (1)	−0.1772 (5)	10.1 (5)[b]
C(44)	0.147 (1)	−0.560 (1)	−0.1613 (5)	8.5 (4)[b]
C(45)	0.239 (1)	−0.485 (1)	−0.1391 (4)	7.9 (4)[b]
C(46)	0.253 (1)	−0.368 (1)	−0.1312 (4)	6.8 (4)[b]
C(51)	−0.0423 (8)	−0.0553 (9)	−0.1279 (3)	4.5 (2)[b]
C(52)	−0.1561 (9)	−0.127 (1)	−0.1416 (4)	5.3 (3)[b]
C(53)	−0.252 (1)	−0.163 (1)	−0.1156 (4)	7.1 (3)[b]
C(54)	−0.235 (1)	−0.134 (1)	−0.0744 (5)	7.8 (4)[b]
C(55)	−0.126 (1)	−0.060 (1)	−0.0601 (4)	7.4 (4)[b]
C(56)	−0.028 (1)	−0.0215 (9)	−0.0867 (4)	6.0 (3)[b]
H(1)	0.194 (7)	0.024 (6)	−0.101 (3)	2 (2)[b]

[a] Numbers in parentheses are estimated standard deviations in the least significant digits in this and all subsequent tables. Anisotropically refined atoms are given in the form of the equivalent isotropic displacement parameter defined as $^4/_3[a^2\beta_{11} + b^2\beta_{22} + c^2\beta_{33} + ab(\cos\gamma)\beta_{12} + ac(\cos\beta)\beta_{13} + bc(\cos\alpha)\beta_{23}]$. Parameters for solvent molecules may be found in the supplementary material. [b] Refined isotropically.

Table IV. Selected Distances (Å) in $[Ir_2(H)_2(CO)_2(\mu\text{-SiPh}_2)(dppm)_2]\cdot 2THF$ (4)[a]

(a) Bonded			
Ir–Ir′	2.8361 (9)	P(1)–C(11)	1.87 (1)
Ir–P(1)	2.340 (3)	P(1)–C(21)	1.85 (1)
Ir–P(2′)	2.344 (3)	P(2)–C(2)	1.81 (1)
Ir–Si	2.371 (4)	P(2)–C(31)	1.83 (1)
Ir–C(1)	1.85 (1)	P(2)–C(41)	1.85 (1)
Ir–H(1)	1.63 (9)	Si–C(51)	1.88 (1)
P(1)–C(2)	1.83 (1)	O(1)–C(1)	1.14 (1)
(b) Nonbonded			
P(1)···P(2)	3.062 (3)	Si···H(1)	2.53 (9)

[a] Additional distances are given in the supplementary material.

(12) Doedens, R. J.; Ibers, J. A. *Inorg. Chem.* **1967**, *6*, 204.
(13) Walker, N.; Stuart, D. *Acta Crystallogr., Sect. A: Found. Crystallogr.* **1983**, *A39*, 1581.
(14) Programs used were those of the Enraf-Nonius Structure Determination Package by B. A. Frenz, in addition to local programs by R. G. Ball.
(15) Cromer, D. T.; Waber, J. T. *International Tables for Crystallography*; Kynoch Press: Birmingham, England, 1974; Vol. IV, Table 2.2A.
(16) Stewart, R. F.; Davidson, E. R.; Simpson, W. T. *J. Chem. Phys.* **1965**, *42*, 3175.
(17) Cromer, D. T.; Liberman, D. *J. Chem. Phys.* **1970**, *53*, 1891.

Table V. Selected Angles (deg) in $[Ir_2(H)_2(CO)_2(\mu\text{-}SiPh_2)(dppm)_2]\cdot 2THF$ (4)[a]

(a) Bond Angles

Ir'-Ir-P(1)	94.51 (7)	Ir-P(1)-C(21)	123.9 (4)
Ir'-Ir-P(2')	84.50 (7)	C(2)-P(1)-C(11)	102.7 (5)
Ir'-Ir-Si	53.26 (6)	C(2)-P(1)-C(21)	102.4 (5)
Ir'-Ir-C(1)	153.1 (5)	C(11)-P(1)-C(21)	100.5 (5)
Ir'-Ir-H(1)	92 (3)	Ir-P(2')-C(2')	110.8 (4)
P(1)-Ir-P(2')	100.6 (1)	Ir-P(2')-C(31')	119.0 (4)
P(1)-Ir-Si	134.82 (8)	Ir-P(2')-C(41')	117.2 (4)
P(1)-Ir-C(1)	110.3 (4)	C(2)-P(2)-C(31)	105.8 (5)
P(1)-Ir-H(1)	75 (3)	C(2)-P(2)-C(41)	103.6 (5)
P(2')-Ir-Si	105.78 (8)	C(31)-P(2)-C(41)	98.7 (5)
P(2')-Ir-C(1)	100.4 (4)	Ir-Si-Ir'	73.5 (1)
P(2')-Ir-H(1)	174 (3)	Ir-Si-C(51)	117.3 (3)
Si-Ir-C(1)	100.3 (5)	Ir-Si-C(51')	127.7 (4)
Si-Ir-H(1)	76 (3)	C(51)-Si-C(51')	96.4 (7)
C(1)-Ir-H(1)	84 (3)	Ir-C(1)-O(1)	176 (1)
Ir-P(1)-C(2)	110.7 (4)	P(1)-C(2)-P(2)	114.3 (6)
Ir-P(1)-C(11)	114.3 (4)		

(b) Torsion Angles

P(1)-Ir-Ir'-P(1')	31.1 (1)
H(1)-Ir-Ir'-H(1')	141 (5)

[a] Additional bond angles are given in the Supplementary Material.

available as supplementary material.

Results and Discussion

Description of Structures. (a) $[Ir_2(H)_2(CO)_2(\mu\text{-}SiPh_2)(dppm)_2]\cdot 2THF$ (4). Complex **4** has the structure shown in Figure 1, in which the molecule contains a crystallographic 2-fold axis of symmetry passing through the Si atom and the center of the Ir–Ir' bond. The metal nuclei are bridged by the two diphosphine ligands and the diphenylsilylene group, but the most striking feature is the

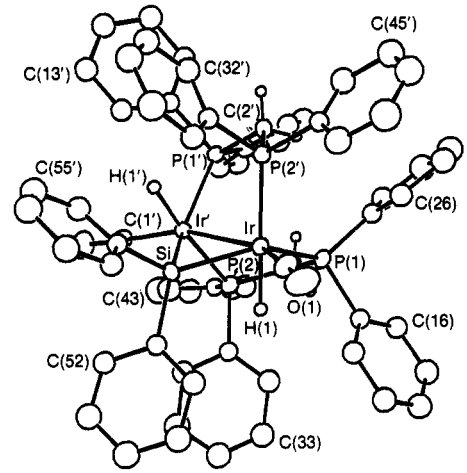

Figure 1. Perspective view of $[Ir_2(H)_2(CO)_2(\mu\text{-}SiPh_2)(dppm)_2]$ (**4**) showing the numbering scheme. Thermal parameters are shown at the 20% level except for hydrogens, which are shown artificially small for the methylene groups but are not shown at all for the phenyl groups.

disposition of the dppm ligands about each metal center. Figure 2 shows a slightly different spatial orientation, with only the ipso carbons of each phenyl ring shown. The atoms P(1) and P(2') are in an approximately cis arrangement about Ir (P(1)–Ir–P(2') = 100.6 (2)°) with P(1) cis to H(1) (P(1)–Ir–H(1) = 75 (3)°) and P(2') trans to H(1) (P(2')–Ir–H(1) = 174 (3)°). This cis-diphosphine arrangement is in contrast with the trans-diphosphine geometry normally observed for binuclear bis-dppm-bridged species but is not without precedent. The complexes $[Rh_2(CO)_2(\mu\text{-}SiHR)_2(dppm)_2]$ (R = Ph,[10a] Et[10b]), $[Rh_2$-

Table VI. Positional and Thermal Parameters of the Atoms of $[Ir_2(H)_2(CO)_2(\mu\text{-}SiHPh)(dppm)_2]\cdot 2THF$ (5)[a]

atom	x	y	z	B, Å²	atom	x	y	z	B, Å²
Ir(1)	0.17446 (8)	−0.03226 (5)	0.31990 (4)	3.06 (2)	C(45)	0.292 (3)	0.151 (2)	0.085 (1)	9 (1)[b]
Ir(2)	0.33528 (8)	0.06018 (5)	0.29519 (4)	3.28 (2)	C(46)	0.263 (2)	0.108 (2)	0.123 (1)	7.2 (8)[b]
P(1)	0.0997 (5)	−0.0471 (3)	0.2347 (3)	3.6 (2)	C(51)	−0.086 (2)	0.039 (1)	0.3315 (9)	4.2 (6)[b]
P(2)	0.2982 (6)	0.0266 (4)	0.2109 (3)	3.9 (2))	C(52)	−0.127 (2)	−0.013 (1)	0.362 (1)	4.9 (6)[b]
P(3)	0.0616 (5)	0.0526 (3)	0.3408 (3)	3.4 (2)	C(53)	−0.242 (2)	−0.024 (1)	0.360 (1)	6.3 (7)[b]
P(4)	0.2134 (5)	0.1470 (3)	0.2960 (3)	3.4 (2)	C(54)	−0.313 (2)	0.011 (2)	0.325 (1)	6.9 (8)[b]
Si	0.3269 (6)	0.0066 (4)	0.3732 (3)	3.6 (2)	C(55)	−0.276 (2)	0.056 (1)	0.295 (1)	6.3 (8)[b]
O(1)	0.092 (2)	−0.138 (1)	0.3824 (7)	7.1 (6)	C(56)	−0.162 (2)	0.073 (1)	0.299 (1)	4.2 (6)[b]
O(2)	0.523 (1)	0.154 (1)	0.3081 (8)	7.3 (6)	C(61)	0.078 (2)	0.083 (1)	0.4085 (9)	3.4 (5)[b]
C(1)	0.123 (2)	−0.100 (1)	0.356 (1)	5.3 (7)	C(62)	0.106 (2)	0.038 (1)	0.446 (1)	4.8 (6)[b]
C(2)	0.456 (2)	0.114 (1)	0.305 (1)	6.0 (8)	C(63)	0.110 (2)	0.060 (1)	0.496 (1)	5.5 (7)[b]
C(3)	0.154 (2)	0.010 (1)	0.1916 (8)	3.4 (6)	C(64)	0.092 (2)	0.125 (1)	0.508 (1)	6.0 (7)[b]
C(4)	0.071 (2)	0.125 (1)	0.3008 (8)	2.9 (6)	C(65)	0.065 (2)	0.170 (1)	0.469 (1)	6.5 (8)[b]
C(11)	−0.049 (2)	−0.041 (1)	0.2149 (9)	4.4 (6)[b]	C(66)	0.052 (2)	0.151 (1)	0.417 (1)	5.2 (7)[b]
C(12)	−0.096 (2)	0.002 (1)	0.178 (1)	5.6 (7)[b]	C(71)	0.241 (2)	0.209 (1)	0.3463 (9)	3.5 (5)[b]
C(13)	−0.213 (3)	0.002 (2)	0.164 (1)	8.2 (9)[b]	C(72)	0.316 (2)	0.197 (1)	0.388 (1)	4.6 (6)[b]
C(14)	−0.271 (2)	−0.042 (2)	0.191 (1)	7.1 (8)[b]	C(73)	0.338 (2)	0.242 (1)	0.428 (1)	6.0 (7)[b]
C(15)	−0.229 (2)	−0.081 (1)	0.227 (1)	5.8 (7)[b]	C(74)	0.282 (2)	0.300 (1)	0.426 (1)	6.3 (8)[b]
C(16)	−0.116 (2)	−0.081 (1)	0.239 (1)	5.2 (7)[b]	C(75)	0.206 (2)	0.312 (1)	0.384 (1)	5.5 (7)[b]
C(21)	0.123 (2)	−0.128 (1)	0.2081 (9)	3.6 (6)[b]	C(76)	0.186 (2)	0.267 (1)	0.344 (1)	4.7 (6)[b]
C(22)	0.175 (2)	−0.178 (1)	0.239 (1)	6.7 (8)[b]	C(81)	0.201 (2)	0.201 (1)	0.2406 (9)	3.9 (6)[b]
C(23)	0.195 (3)	−0.238 (2)	0.216 (1)	8.2 (9)[b]	C(82)	0.107 (2)	0.217 (1)	0.211 (1)	6.2 (8)[b]
C(24)	0.163 (2)	−0.250 (1)	0.164 (1)	6.8 (8)[b]	C(83)	0.100 (3)	0.259 (2)	0.166 (1)	7.9 (9)[b]
C(25)	0.109 (3)	−0.203 (2)	0.136 (1)	7.7 (9)[b]	C(84)	0.192 (2)	0.283 (2)	0.158 (1)	6.6 (8)[b]
C(26)	0.090 (2)	−0.140 (1)	0.157 (1)	5.5 (7)[b]	C(85)	0.287 (2)	0.272 (1)	0.187 (1)	6.2 (8)[b]
C(31)	0.365 (2)	−0.051 (1)	0.1929 (9)	4.1 (6)[b]	C(86)	0.290 (2)	0.231 (1)	0.229 (1)	5.3 (7)[b]
C(32)	0.352 (2)	−0.067 (2)	0.142 (1)	6.9 (8)[b]	C(91)	0.436 (2)	−0.053 (1)	0.3971 (9)	3.9 (6)[b]
C(33)	0.402 (3)	−0.127 (2)	0.129 (1)	9 (1)[b]	C(92)	0.512 (2)	−0.038 (1)	0.4379 (9)	4.4 (6)[b]
C(34)	0.461 (3)	−0.164 (2)	0.162 (1)	8.0 (9)[b]	C(93)	0.596 (2)	−0.076 (1)	0.462 (1)	5.4 (7)[b]
C(35)	0.470 (3)	−0.145 (2)	0.211 (1)	8.1 (9)[b]	C(94)	0.596 (2)	−0.137 (1)	0.440 (1)	6.0 (7)[b]
C(36)	0.424 (2)	−0.087 (1)	0.226 (1)	5.9 (7)[b]	C(95)	0.531 (3)	−0.158 (2)	0.399 (1)	7.2 (8)[b]
C(41)	0.336 (2)	0.084 (1)	0.161 (1)	5.1 (7)[b]	C(96)	0.444 (2)	−0.114 (1)	0.379 (1)	5.5 (7)[b]
C(42)	0.446 (2)	0.094 (2)	0.165 (1)	7.2 (8)[b]	H(1)[c]	0.2727	−0.0867	0.3145	4.0
C(43)	0.485 (3)	0.133 (2)	0.127 (1)	11 (1)[b]	H(2)[c]	0.4021	−0.0126	0.2869	4.0
C(44)	0.410 (3)	0.158 (2)	0.093 (1)	8 (1)[b]					

[a] See footnote *a* of Table III. [b] Refined isotropically. [c] Fixed contribution; not refined.

Table VII. Selected Distances (Å) in $[Ir_2(H)_2(CO)_2(\mu\text{-SiHPh})(dppm)_2]\cdot 2THF$ (5)

(a) Bonded			
Ir(1)-Ir(2)	2.879 (1)	P(1)-C(21)	1.84 (2)
Ir(1)-P(1)	2.344 (5)	P(2)-C(3)	1.83 (2)
Ir(1)-P(3)	2.331 (4)	P(2)-C(31)	1.88 (2)
Ir(1)-Si	2.343 (5)	P(2)-C(41)	1.87 (2)
Ir(1)-C(1)	1.84 (2)	P(3)-C(4)	1.82 (2)
Ir(1)-H(1)	1.67	P(3)-C(51)	1.85 (2)
Ir(2)-P(2)	2.322 (5)	P(3)-C(61)	1.88 (2)
Ir(2)-P(4)	2.324 (5)	P(4)-C(4)	1.84 (2)
Ir(2)-Si	2.349 (5)	P(4)-C(71)	1.83 (2)
Ir(2)-C(2)	1.85 (2)	P(4)-C(81)	1.82 (2)
Ir(2)-H(2)	1.72	Si-C(91)	1.87 (2)
P(1)-C(3)	1.83 (2)	O(1)-C(1)	1.13 (2)
P(1)-C(11)	1.86 (2)	O(2)-C(2)	1.16 (2)
(b) Nonbonded			
P(1)···P(2)	3.02 (1)	Si···H(1)	2.48
P(3)···P(4)	3.04 (1)	Si···H(2)	2.61

[a] Additional distances are given in the supplementary material.

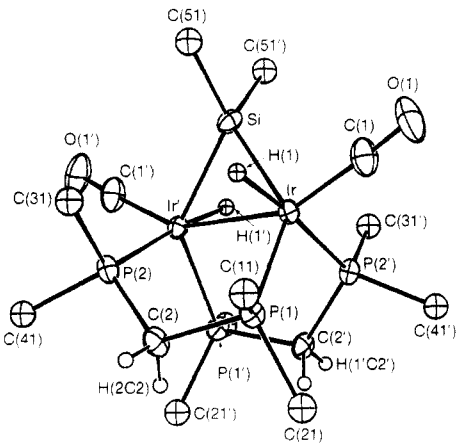

Figure 2. View of complex **4** omitting the phenyl carbon atoms except those bound to phosphorus and silicon.

$(CO)_2(\mu\text{-}\eta^2\text{-PhCCPh})(dppm)_2]$,[18] $[Ir_2(CO)_2(\mu\text{-}\eta^2\text{-}MeO_2CC{\equiv}CCO_2Me)(dppm)_2]$,[19] and $[Pt_2Me_4(dRpm)_2]$ (R = Ph (dppm), Me (dmpm))[20] all possess structures in which the phosphine–metal–phosphine angles deviate significantly from linearity at both metal centers, while $[Pt_2Me_3(dppm)_2]^+$,[21] $[Rh_2(CO)_3(dppm)_2]$,[22] $[RhIr(CO)_3(dppm)_2]$,[7] and the related $[Rh_2(CO)_3\{(PhO)_2PN(Et)P(OPh)_2\}_2]$[23] and $[Rh_2Cl_2(CO)\{(PhO)_2PN(Et)P(OPh)_2\}_2]$[24] have cis phosphines at one metal center and trans phosphines at the other. The coordination geometry about Ir in complex **4** appears to be roughly octahedral, with the six sites occupied by C(1), Ir′, P(1), P(2′), H(1), and Si. The distortions from the idealized geometry result primarily from the constraints imposed by the bridging diphenylsilylene group (e.g. Ir–Ir′–Si = 53.26 (6)°, P(1)–Ir–Si = 134.82 (2)°, Si–Ir–H(1) = 76 (3)°).

The disposition of the silylene and hydride groups with respect to each other is consistent with a concerted oxidative addition of a silicon–hydrogen bond to each metal center, the Si and H atoms being approximately cis about

Table VIII. Selected Angles (deg) in $[Ir_2(H)_2(CO)_2(\mu\text{-SiHPh})(dppm)_2]\cdot 2THF$ (5)[a]

(a) Bond Angles			
Ir(2)-Ir(1)-P(1)	93.6 (1)	P(4)-Ir(2)-Si	103.8 (2)
Ir(2)-Ir(1)-P(3)	91.8 (1)	P(4)-Ir(2)-C(2)	93.8 (6)
Ir(2)-Ir(1)-Si	52.3 (1)	P(4)-Ir(2)-H(2)	167.5
Ir(2)-Ir(1)-C(1)	154.7 (6)	Si-Ir(2)-C(2)	106.2 (7)
Ir(2)-Ir(1)-H(1)	82.8	Si-Ir(2)-H(2)	78.1
P(1)-Ir(1)-P(3)	98.6 (2)	C(2)-Ir(2)-H(2)	97.6
P(1)-Ir(1)-Si	144.0 (2)	Ir(1)-P(1)-C(3)	112.9 (5)
P(1)-Ir(1)-C(1)	106.8 (6)	Ir(1)-P(1)-C(11)	121.1 (6)
P(1)-Ir(1)-H(1)	92.1	Ir(1)-P(1)-C(21)	115.0 (6)
P(3)-Ir(1)-Si	94.2 (2)	C(3)-P(1)-C(11)	102.9 (8)
P(3)-Ir(1)-C(1)	99.5 (7)	C(3)-P(1)-C(21)	103.8 (8)
P(3)-Ir(1)-H(1)	168.4	C(11)-P(1)-C(21)	98.9 (8)
Si-Ir(1)-C(1)	104.0 (6)	Ir(2)-P(2)-C(3)	112.7 (5)
Si-Ir(1)-H(1)	74.4	Ir(2)-P(2)-C(31)	117.0 (6)
C(1)-Ir(1)-H(1)	81.9	Ir(2)-P(2)-C(41)	117.4 (7)
Ir(1)-Ir(2)-P(2)	88.4 (1)	C(3)-P(2)-C(31)	103.1 (8)
Ir(1)-Ir(2)-P(4)	91.1 (1)	C(3)-P(2)-C(41)	104.2 (8)
Ir(1)-Ir(2)-Si	52.1 (1)	C(31)-P(2)-C(41)	100.5 (8)
Ir(1)-Ir(2)-C(2)	158.3 (7)	Ir(1)-P(3)-C(4)	111.5 (5)
P(2)-Ir(2)-Si	133.2 (2)	Ir(1)-P(3)-C(51)	118.7 (6)
P(2)-Ir(2)-C(2)	111.4 (7)	Ir(1)-P(3)-C(61)	118.3 (5)
P(2)-Ir(2)-H(2)	70.3	C(4)-P(3)-C(51)	100.6 (8)
Ir(1)-Ir(2)-H(2)	80.3	C(4)-P(3)-C(61)	106.5 (7)
P(2)-Ir(2)-P(4)	100.7 (2)	C(51)-P(3)-C(61)	99.2 (7)
Ir(2)-P(4)-C(4)	116.4 (5)	Ir(1)-Si-C(91)	118.8 (6)
Ir(2)-P(4)-C(71)	117.9 (6)	Ir(2)-Si-(C(91)	118.9 (6)
Ir(2)-P(4)-C(81)	115.6 (6)	Ir(1)-C(1)-O(1)	174 (2)
C(4)-P(4)-C(71)	102.0 (7)	Ir(2)-C(2)-O(2)	172 (2)
C(4)-P(4)-C(81)	102.8 (8)	P(1)-C(3)-P(2)	111.9 (8)
C(71)-P(4)-C(81)	99.6 (8)	P(3)-C(4)-P(4)	112.1 (8)
Ir(1)-Si-Ir(2)	75.7 (2)		

(b) Torsion Angles	
P(1)-Ir(1)-Ir(2)-P(2)	14.7 (2)
P(3)-Ir(1)-Ir(2)-P(4)	12.7 (2)
H(1)-Ir(1)-Ir(2)-H(2)	6.6

[a] Additional bond angles are given in the supplementary material.

Ir. The hydrides are disposed roughly trans to each other on adjacent metals with a torsion angle about the Ir–Ir′ bond (H(1)–Ir–Ir′–H(1′)) of 141 (5)° and thus are located on opposite faces of the plane defined by the Ir, Ir′ and Si atoms. Unlike some other binuclear silylene-bridged hydride complexes, where three-center–two-electron Si–H–M bonding is implicated,[25] compound **4** does not appear to show significant Si–H interaction. Although the Si–H(1) distance (2.53 (9) Å) is well within the sum of the van der Waals radii of these atoms (3.30–3.55 Å),[26] this arrangement appears to be enforced by the pseudooctahedral geometry of the complex and not by any silicon–hydrogen bonding. Schubert has proposed, as a criterion for agostic Si–H bonding, an upper limit of 2.0 Å for the silicon–hydrogen distance;[25] this limit is based on the longest accepted interatomic distances for Si–Si and H–H bonds. This proposal is supported by several crystallographic studies in which the Si–H distances for agostic Si–H···M interactions fall within the range 1.56–1.80 Å. The hydride ligand, H(1), was refined acceptably, and the resulting Ir–H(1) distance (1.63 (9) Å) corresponds to a normal covalent bond. This hydride does not appear to display a significant trans influence, as seen in the essentially identical iridium–phosphorus bond lengths (Ir–P(1) = 2.340 (3) Å; Ir–P(2′) = 2.344 (3) Å).

The Ir–Si bond length of 2.371 (4) Å is slightly shorter than the range reported for several related silane com-

(18) Berry, D. H.; Eisenberg, R. *Organometallics* **1987**, *6*, 1796.
(19) McDonald, R.; Cowie, M. Manuscript in preparation.
(20) Manojlović-Muir, L.; Muir, K. A.; Frew, A. A.; Ling, S. S. M.; Thomson, M. A.; Puddephatt, R. J. *Organometallics* **1984**, *3*, 1637.
(21) Brown, M. P.; Cooper, S. J.; Frew, A. A.; Manojlović-Muir, L.; Muir, K. A.; Puddephatt, R. J.; Seddon, K. R.; Thomson, M. A. *Inorg. Chem.* **1981**, *20*, 1500.
(22) Woodcock, C.; Eisenberg, R. *Inorg. Chem.* **1985**, *24*, 1285.
(23) Haines, R. J.; Meintjies, E.; Laing, M.; Sommerville, P. *J. Organomet. Chem.* **1981**, *216*, C19.
(24) Haines, R. J.; Meintjies, E.; Laing, M. *Inorg. Chim. Acta* **1979**, *36*, L403.
(25) Schubert, U. *Adv. Organomet. Chem.*, in press, and references therein.
(26) Huheey, J. E. *Inorganic Chemistry*, 3rd ed.; Harper and Row: New York, 1983; pp 258–259, and references therein.

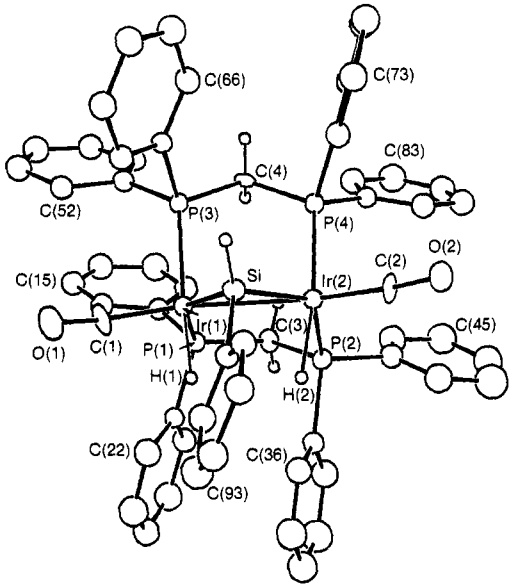

Figure 3. Perspective view of $[Ir_2(H)_2(CO)_2(\mu\text{-SiHPh})(dppm)_2]$ (**5**) showing the numbering scheme. Thermal parameters are shown at the 20% level except for hydrogens, which are shown artificially small for the hydride, silylene, and methylene groups but are not shown at all for the phenyl groups.

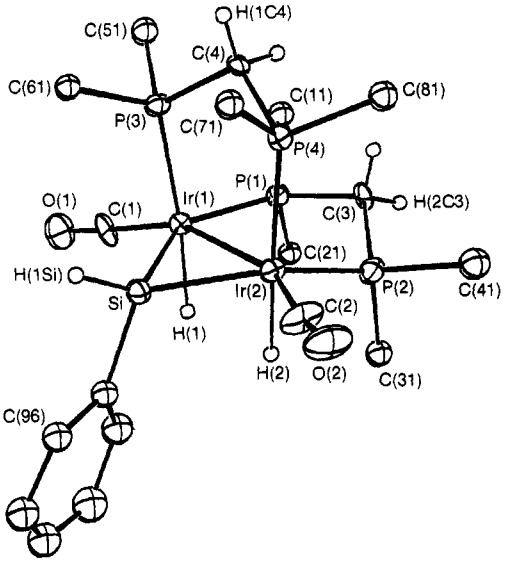

Figure 4. View of complex **5** omitting the dppm phenyl carbon atoms except those bound to phosphorus. The positions shown for H(1) and H(2) are approximate (see text).

plexes (2.390–2.454 Å)[27] but is not unusual, since it appears to be a general phenomenon that metal–silicon distances are shorter in complexes containing bridging silylene groups as compared to those featuring terminal silyl groups.[4] One exception is $(Me_3P)_3Ir(SiMeCl_2)Cl_2$, for which the Ir–Si distance (2.299 (5) Å)[28] is even shorter than in the present compound. However, this is believed to be due to the high electron density on the Ir center of this species, coupled with the better π-acceptor ability of the $SiMeCl_2$ group.[28] The acute Ir–Si–Ir′ angle of 73.5 (1)° is within the expected range for such a unit that spans a metal–metal bond. Overall the Ir_2Si unit has structural parameters very similar to those found for the Rh_2Si units of the complexes $[Rh(CO)(\mu\text{-SiHR})(dppm)]_2$ (R = Ph, Et).[10]

Complex **4** is twisted significantly about the Ir–Ir bond, resulting in a staggered arrangement of P(1) and P(2), as shown by the P(1)–Ir–Ir′–P(2) torsion angle of 31.1 (1)°. Furthermore, the bridging silylene group is twisted relative to the metals (Ir–Si–C(51) = 117.3 (3)°; Ir–Si–C(51′) = 127.7 (4)°) such that the phenyl group containing C(51) is rotated into the less congested space in the vicinity of the small hydride ligand, H(1).

The Ir–Ir′ separation (2.8361 (9) Å) is consistent with a normal single bond and is within the range observed for similar diiridium systems (2.7661–2.8933 Å);[6,9,11,29] as a result, the metal–metal distance is compressed with respect to the intraligand P–P separation (P(1)···P(2) = 3.062 (3) Å). The carbonyl group, C(1)O(1), does not lie exactly along the metal–metal bond axis (Ir′–Ir–C(1) = 153.1 (5)°), presumably reflecting the distortion of the complex by the acute bite of the bridging diphenylsilylene group.

(b) $[Ir_2(H)_2(CO)_2(\mu\text{-SiHPh})(dppm)_2]\cdot 2THF$ (5). The structure of **5** is shown in Figure 3, while Figure 4 presents an alternate orientation, in which only the ipso carbons of the dppm phenyls are shown. Similar to the case for complex **4**, the iridium centers are bridged by the phenylsilylene group, while the diphosphine groups have a cis disposition on each metal (P(1)–Ir(1)–P(3) = 98.6 (2)°; P(2)–Ir(2)–P(4) = 100.7 (2)°). Although, as noted earlier, the hydride positions in **5** were not unambiguously located in the X-ray study, they are included in the positions derived from the Fourier map. These positions are in complete agreement with the spectroscopic data (vide infra) and with the locations of the other atoms in the structure, which leave obvious coordination sites in the positions of these hydrides. Their positions on each metal are also consistent with those in complex **4**, for which the hydride parameters were successfully refined. Since the hydride positions in **5** are estimated, bond lengths and angles involving these atoms are necessarily approximate but are nevertheless in excellent agreement with the corresponding parameters for **4**. One hydride ligand on each metal is located cis to one phosphine (P(1)–Ir(1)–H(1) ≅ 92°; P(2)–Ir(2)–H(2) ≅ 70°) and trans to another (P(3)–Ir(1)–H(1) and P(4)–Ir(2)–H(2) ≅ 168°) as in **4**, and again the metal–phosphorus distances are apparently unaffected by the presence of the hydrides (Ir(1)–P(1) = 2.344 (5) Å; Ir(1)–P(3) = 2.331 (4) Å; Ir(2)–P(2) = 2.322 (5) Å; Ir(2)–P(4) = 2.324 (5) Å). The hydride ligands are also situated cis to the bridging phenylsilylene group, giving Si–Ir(1)–H(1) and Si–Ir(2)–H(2) angles of ca. 74 and 78°, respectively, and silicon–hydride distances of Si···H(1) ≅ 2.5 Å and Si···H(2) ≅ 2.6 Å. Again, the relatively close proximity of the Si and H atoms is not believed to indicate a significant interaction above that imposed by the geometry of the complex. The geometry of the Ir(1)–Si–Ir(2) bridge is rather similar to that of compound **4**, having comparable Ir–Si bond lengths (2.343 (5), 2.349 (5) Å) and Ir(1)–Si–Ir(2) angle (75.7 (2)°). Each metal displays an approximately octahedral coordination geometry, with a CO group, the other iridium center, two phosphines, the phenyl-

(27) (a) Curtis, M. D.; Greene, J.; Butler, W. M. *J. Organomet. Chem.* **1979**, *164*, 371. (b) Auburn, M. J.; Grundy, S. L.; Stobart, S. R.; Zawortko, M. J. *J. Am. Chem. Soc.* **1985**, *107*, 266. (c) Ricci, J. S., Jr.; Koetzle, T. F.; Fernández, M.-J.; Maitlis, P. M.; Green, J. C. *J. Organomet. Chem.* **1986**, *299*, 383. (d) Fernández, M.-J.; Esteruelas, M. A.; Oro, L. A.; Apreda, M.-C.; Foces-Foces, C.; Cano, F. H. *Organometallics* **1987**, *6*, 1751. (e) Rappoli, B. J.; Janik, T. S.; Churchill, M. R.; Thompson, J. S.; Atwood, J. D. *Organometallics* **1988**, *7*, 1939.

(28) Zlota, A. A.; Frolow, F.; Milstein, D. *J. Chem. Soc., Dalton Trans.* **1989**, 1826.

(29) (a) Kubiak, C. P.; Woodcock, C.; Eisenberg, R. *Inorg. Chem.* **1980**, *19*, 2733. (b) Sutherland, B. R.; Cowie, M. *Inorg. Chem.* **1984**, *23*, 2324. (c) Mague, J. T.; Klein, C. L.; Majeste, R. J.; Stevens, E. D. *Organometallics* **1984**, *3*, 1860. (d) Sutherland, B. R.; Cowie, M. *Organometallics* **1984**, *3*, 1869. (e) Wu, J.; Reinking, M. K.; Fanwick, P. E.; Kubiak, C. P. *Inorg. Chem.* **1987**, *26*, 247. (f) Wu, J.; Fanwick, P. E.; Kubiak, C. P. *Organometallics* **1987**, *6*, 1805. (g) Balch, A. L.; Waggoner, K. M.; Olmstead, M. M. *Inorg. Chem.* **1988**, *27*, 4511.

silylene group, and a hydride acting as ligands. Deviations from this geometry, especially the offset of the otherwise normal terminal CO's from the Ir(1)–Ir(2) axis (Ir(2)–Ir(1)–C(1) = 154.7 (6)°; Ir(1)–Ir(2)–C(2) = 158.3 (7)°), appear to again result from the acute bite angle of the silylene bridge.

The phosphorus atoms belonging to the same dppm ligands in **5** are much closer to being eclipsed (P(1)–Ir(1)–Ir(2)–P(2) torsion 14.7 (2)°; P(3)–Ir(1)–Ir(2)–P(4) torsion 12.7 (2)°) than those of **4**, and the hydrides are now on the same side of the Ir(1)–Ir(2)–Si plane, with the Ir–H vectors approximately parallel. In addition, the silylene bridge of **5** appears not to show twisting at the silicon atom (Ir(1)–Si–C(91) = 118.8 (6)°; Ir(2)–Si–C(91) = 118.9 (6)°), indicating much less steric interaction between the silylene phenyl group and the dppm phenyls than was observed in **4**. It can be seen that while the phenylsilylene group is closer to one dppm group (P(3)–Ir(1)–Si = 94.2 (2)°; P(4)–Ir(2)–Si = 103.8 (2)°) than the other (P(1)–Ir(1)–Si = 144.0 (2)°; P(2)–Ir(2)–Si = 133.2 (2)°) its phenyl ring is held on the opposite side of the Ir(1)–Si–Ir(2) plane from the proximal (P(3)–C(4)–P(4)) dppm ligand and is instead oriented toward the small hydride ligands.

The Ir(1)–Ir(2) distance of 2.879 (1) Å is very close to that of **4** and is again shorter than the intraligand P···P separations (P(1)···P(2) = 3.02 (1) Å; P(3)···P(4) = 3.04 (1) Å), indicating a mutual attraction of the two metals.

Preparation and Characterization of Compounds. Although the dialkylsilylene-, diphenylsilylene-, and phenylsilylene-bridged dimers **2–5** each possess several unique features, it is helpful to first characterize them in terms of their similarities. Each complex is formed via oxidative addition of an Si–H bond of a primary or secondary silane to each of the metal centers of $[Ir_2(CO)_3(dppm)_2]$, with concomitant loss of a CO ligand. The reactions are facile under ambient conditions, yielding compounds containing terminal carbonyl and hydride groups on each iridium and a silylene bridge between the metals. Structurally these species are reminiscent of the previously reported series of compounds $[Rh_2(H)_2(CO)_2(\mu\text{-}SiRR')(dppm)_2]$ (R = H, R′ = Et, Ph, *n*-hexyl; R = Me, R′ = Ph; R = R′ = Me, Et)[10] and $[Re_2(CO)_8(H)_2(\mu\text{-}SiPh_2)]$.[30] However, they display some notable differences in reactivity compared to that of their rhodium analogues. Unlike the Rh species, complexes **2–5** cannot be induced to reductively substitute CO for H_2. These diiridium species remain unchanged under carbon monoxide, even in refluxing THF, and do not yield any carbonyl-bridged, hydride-free products as observed for the dirhodium compounds. This inability to lose H_2 is also in contrast to the behavior of the related A-frame dihydride $[Ir_2(H)_2(CO)_2(\mu\text{-}S)(dppm)_2]$, which, under reflux in THF or over time under N_2, loses H_2 to form $[Ir_2(CO)_2(\mu\text{-}S)(dppm)_2]$.[31] The μ-SiR_2 complexes **2–4** are thermally stable in the solid state and in solution and, unlike their dirhodium counterparts, do not react further by P–C bond cleavage and P–Si bond formation to yield products analogous to $[Rh_2(CO)_2(\mu\text{-}H)(dppm)(Ph_2PCH_2PPhSiRR')]$.[10] In addition, complex **5** is not fluxional and does not react with a second equivalent of $PhSiH_3$, whereas the compounds $[Rh_2(H)_2(CO)_2(\mu\text{-}SiHR)(dppm)_2]$ (R = Et, Ph) rapidly undergo hydride exchange between the Rh and Si centers at room temperature and react with $RSiH_3$ to yield $[Rh_2(CO)_2(\mu\text{-}SiHR)_2(dppm)_2]$.[10]

(30) (a) Hoyano, J. K.; Elder, M.; Graham, W. A. G. *J. Am. Chem. Soc.* **1969**, *91*, 4568. (b) Elder, M. *Inorg. Chem.* **1970**, *9*, 762.
(31) Vaartstra, B. A.; O'Brien, K. N.; Eisenberg, R.; Cowie, M. *Inorg. Chem.* **1988**, *27*, 3668.

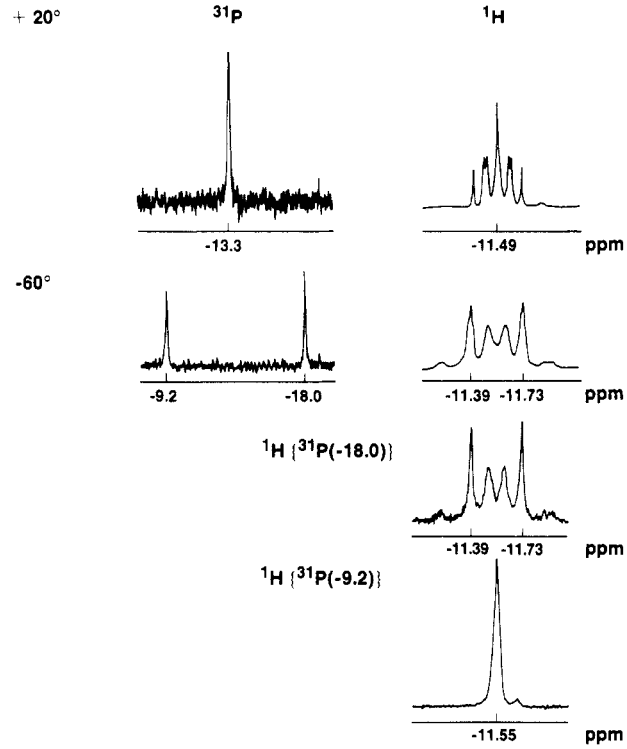

Figure 5. $^{31}P\{^1H\}$, ^1H, and $^1H\{^{31}P\}$ NMR spectra of complex **2** at 20 and −60 °C.

Complexes **2–4** *are* fluxional at room temperature, but in a different manner from their dirhodium analogues; furthermore, the fluxional process involved for compounds **2** and **3** is somewhat different from that for **4** (vide infra). The signals observed at room temperature in the $^{31}P\{^1H\}$ and high-field region of the ^1H NMR spectra of species **2** are shown in Figure 5; the spectra for **3** are quite comparable. The phosphorus NMR spectrum at ambient temperature shows a single broad resonance, implying one time-averaged phosphorus environment, and the proton NMR spectrum shows two different dppm methylene resonances, integrated as two protons each, and one signal in the high-field region, due to the terminal hydrides on iridium. This high-field resonance appears as a second-order multiplet characteristic of an AA′XX′X″X‴ spin system, with an intensity corresponding to two hydrogens. The silylene methyl protons of **2** appear as a single broadened resonance at δ 0.70, while the hydrogens of the $SiEt_2$ group of **3** appear as a single triplet–quartet combination at δ 1.13 and 0.88, respectively.

At −60 °C the NMR spectra of these complexes differ substantially from those observed at room temperature. As shown in Figure 5, the phosphorus spectrum of the dimethylsilylene-bridged complex **2** shows a splitting of the high-temperature singlet into two broadened singlets (at δ −9.2 and −18.0). The corresponding proton spectrum shows four different dppm methylene resonances (at δ 6.33, 6.09, 2.85, and 2.69), integrated as one hydrogen each, and the high-field region again shows a second-order, two-proton signal that now appears as a broadened pattern arising from an AA′XX′YY′ spin system and is centered at δ −11.55. Selective heteronuclear decoupling of the high-field phosphorus resonance produces a sharpening of the spectral lines of the hydride multiplet, while irradiation of the low-field phosphorus signal causes a collapse of the hydride resonance, indicating a larger coupling of the hydride to the low-field than to the high-field phosphorus. Similar effects were observed in the low-temperature NMR spectra of complex **3**. The structural features giving rise

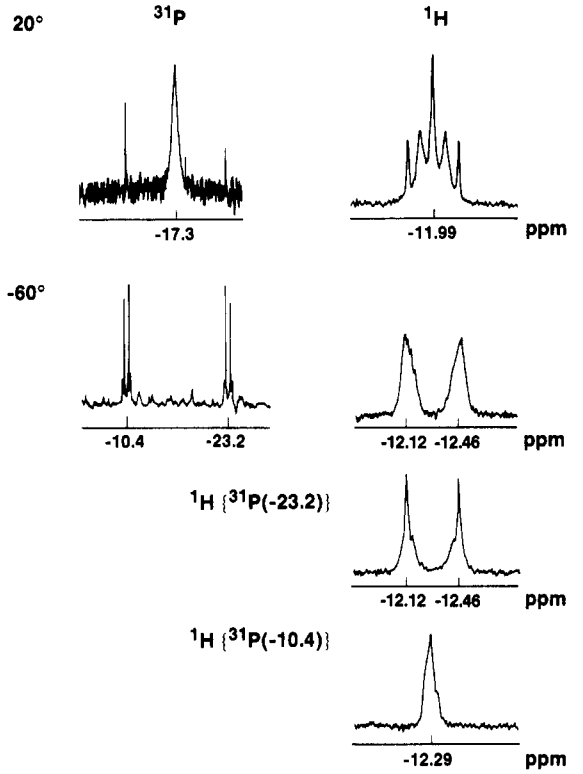

Figure 6. $^{31}P\{^1H\}$, ^1H, and $^1H\{^{31}P\}$ NMR spectra of complex **4** at 20 and −60 °C.

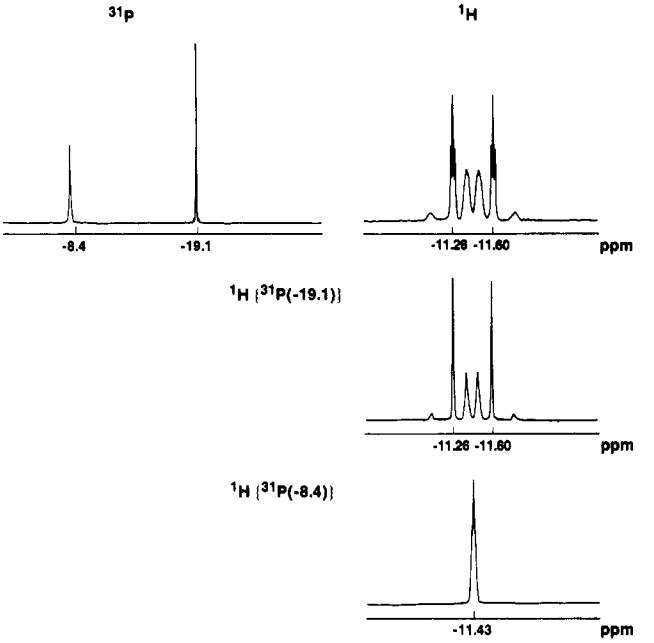

Figure 7. $^{31}P\{^1H\}$, ^1H, and $^1H\{^{31}P\}$ NMR spectra of complex **5** at 20 °C.

to these spectral observations, as well as the mechanism of ambient-temperature fluxionality of **2** and **3**, can be more easily explained in light of the spectra and solid-state structures observed for **4** and **5** (vide infra).

At ambient temperature the NMR spectra for **4** are quite similar to those of **2** and **3**. As shown in Figure 6, the $^{31}P\{^1H\}$ spectrum shows a broad singlet and in the high-field region of the ^1H spectrum there appears a resonance due to a AA′XX′X″X‴ spin system. It is important to note that this latter resonance is not a true first-order (1:4:6:4:1) quintet and so does not necessarily imply a structure in which the hydrides bridge the metals. This resonance resembles that of **2** (Figure 5), except that the broader lines adjacent to the central peak in **4** are resolved into two lines each in **2**. A rather analogous spectrum was observed for the closely related species $[Ir_2(H)_2(CO)_2(\mu\text{-}S)(dppm)_2]$,[31] in which one hydride ligand is terminally bound to each metal.

The low-temperature $^{31}P\{^1H\}$ NMR spectrum of **4** (see Figure 6) also shows a splitting of the room-temperature singlet, but the pattern observed is now an AA′BB′ multiplet, in which the two branches are centered at δ −10.4 and −23.2. Under these conditions, the proton NMR spectrum shows only two resonances attributable to methylene hydrogens (at δ 6.07 and 2.92); this is in agreement with the solid-state structure of **4**, in that the 2-fold symmetry of the molecule would still lead to two sets of two equivalent methylene protons. The high-field region of the proton NMR spectrum again shows a multiplet (centered at δ −12.29) due to the AA′ nuclei of an AA′XX′YY′ spin system, but one very different from those seen for **2** and **3**, here resembling two complex unresolved multiplets. Selective heteronuclear phosphorus decoupling again indicates a larger coupling of the hydrides to the low-field than to the high-field phosphorus atoms, as shown in Figure 6. The two different couplings are consistent with the solid-state structure, which shows that each hydride is trans to one phosphorus nucleus, and therefore more strongly coupled to it, and cis to the other, to which it displays a smaller coupling.

The differences between the low-temperature NMR spectra of **2** and **3** and those of **4** imply that the limiting conformations of the dialkylsilylene-bridged species are different from that adopted by the diphenylsilylene complex. In this context, elucidation of the static structures of **2** and **3** is aided by comparison of their low-temperature proton and phosphorus NMR spectra with the corresponding ambient-temperature spectra of the nonfluxional phenylsilylene-bridged compound **5**, shown in Figure 7. The $^{31}P\{^1H\}$ NMR spectrum of complex **5** shows two slightly broadened resonances (δ −8.4 and −19.1), while the ^1H spectrum shows four different methylene hydrogens (δ 6.39, 6.08, 3.22, and 2.82) and an AA′XX′YY′ spin system multiplet for the hydrides (centered at δ −11.43). Heteronuclear decoupling of the high-field phosphorus resonance causes collapse of the hydride signal to a pattern characteristic of an AA′XX′ spin system, while irradiation of the low-field phosphorus resonance changes the hydride peak to a narrow pseudotriplet; these results are in agreement with the solid-state structure of complex **5**, in that the hydrides would be expected to be more strongly coupled to the phosphorus atoms located trans to them at the iridium center than to the phosphorus in the cis position, as was observed for **4**. The ambient-temperature $^{31}P\{^1H\}$, ^1H, and $^1H\{^{31}P\}$ NMR spectra of **5** are very similar to those observed at −60 °C for species **2** and **3** but are quite different from the corresponding low-temperature spectra of compound **4**. Thus, it appears that the dialkylsilylene-bridged complexes **2** and **3** adopt *static* configurations directly analogous to the crystallographically determined structure of **5** (with SiR_2 groups replacing the SiHPh unit). We propose that the fluxionality observed for the dialkylsilylene-bridged complexes occurs via the process

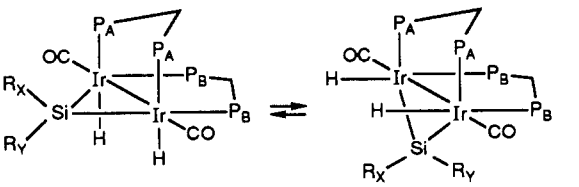

in which the μ-silylene group reversibly migrates from a position opposite the P_B nuclei to a site opposite the P_A nuclei, while the hydride ligands undergo an analogous but opposite interchange (i.e. from trans to P_A to trans to P_B). Rapid exchange between these two limiting forms would result in equilibration of the P_A and P_B phosphorus nuclei and also of the R_X and R_Y alkyl groups. When R_X and R_Y are the same (both Me or both Et), the two conformations shown are energetically equivalent. However, when R_Y is a phenyl group and R_X is a hydrogen, as in complex **5**, the structure shown on the left, in which the bulky silylene phenyl group is held toward the small hydride ligands and away from the bulky diphosphine bridges, would be more favored than that on the right. This is the structure adopted by complex **5**, which is not fluxional at room temperature.

We have carried out simulations of the ambient-temperature ^1H NMR spectra of compounds **2** and **5**. The results for **2** yield information about the time-averaged structure in fluxional process, while those for **5** are characteristic of the static structure. A satisfactory simulation of the hydride resonance of **2** was obtained by employing the values $J_{AA'} = 1.2$ Hz ($^3J_{H-H}$), $J_{AX} = J_{AX''} = J_{A'X'} = J_{A'X'''} = 49.6$ Hz ($^2J_{P-H}$), $J_{AX'} = J_{AX'''} = J_{A'X} = J_{A'X''} = 11.0$ Hz ($^3J_{PH}$), $J_{XX'} = J_{X''X'''} = 133$ Hz (through-backbone $^2J_{P-P}$), $J_{XX''} = J_{X'X'''} = 29$ Hz (through-metal $^2J_{P-P}$), and $J_{XX'''} = J_{X'X''} = -26$ Hz (gauche $^3J_{P-P}$). The hydride resonance of **5** was simulated by using the following values: $J_{AA'} = 4.3$ Hz ($^3J_{H-H}$), $J_{AX} = J_{A'X'} = 125.1$ Hz (trans $^2J_{P-H}$), $J_{AX'} = J_{A'X} = 12.6$ Hz ($^3J_{P-H}$), $J_{AY} = J_{A'Y'} = 7.2$ Hz (cis $^2J_{P-H}$), $J_{AY'} = J_{A'Y} = 5.2$ Hz ($^3J_{P-H}$), $J_{XX'} = 123.9$ Hz (through-backbone $^2J_{P-P}$), $J_{XY} = J_{X'Y'} = 28.8$ Hz (cis $^2J_{P-P}$), $J_{XY'} = J_{X'Y} = -26.2$ Hz (gauche $^3J_{P-P}$), and $J_{YY'} = 141.9$ Hz (through-backbone $^2J_{P-P}$). It should be pointed out that attempted fittings of the spectra of **5** were more successful in the $^1H\{^{31}P\}$ cases than for the undecoupled ^1H spectrum, since the broadness of some of the observed peaks prevented a closer fit of simulation to data. Simulation of the hydride resonance of **2** at −60 °C was not attempted due to the decreased resolution of this signal; however, its close resemblance to the room-temperature hydride resonance of **5** (see Figures 5 and 7) implies that the couplings giving rise to the former pattern will be much the same as those found for the latter. In this light, the fact that the nominally two-bond phosphorus–hydrogen coupling for **2** at room temperature (49.6 Hz) is approximately midway between the trans (125.1 Hz) and cis (7.2 Hz) $^2J_{P-H}$ values for **5** appears to reflect the site exchange taking place, resulting in equivalence of the phosphorus nuclei and averaging of these P–H couplings. According to the mechanism above, the fluxional process occurs via movement of the hydride and silylene groups with respect to the "fixed" Ir_2P_4 core; thus, the values for the through-backbone, through-metal, and gauche P–P couplings should remain relatively constant upon going from the static to the fluxional species, which is indeed the case. Overall, the values obtained are in line with previous results for iridium–phosphorus and diphosphine-bridged systems.[10,32]

A slightly different mode of interchange, in which the complex oscillates between enantiomeric forms of the crystallographically determined structure, would appear to be at work for species **4** and is shown by the Newman projections

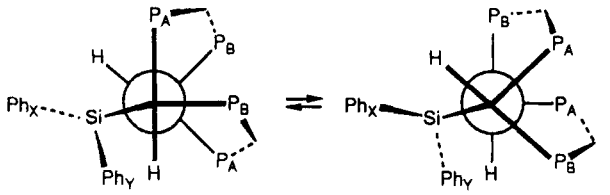

viewed down the Ir–Ir bond. The carbonyl ligands, which would remain equivalent in either limiting configuration, have been omitted for clarity. This mechanism involves a twisting of the P–Ir–P units with respect to each other, an oscillation of the $SiPh_2$ bridge about the molecule's 2-fold axis of symmetry, and movement (while remaining attached to the same metal) of the hydride ligands from positions trans to the P_A phosphorus atoms to opposite the P_B atoms. This is a somewhat more complex mode of interchange than that proposed for **2** and **3**, presumably because of the more severe steric interactions involving the large phenyl substituents on Si and the dppm ligands in **4**, which result in the differing structures as noted previously. In complex **4** interchange of the hydride and silylene positions, in which the hydride ligands migrate to different sides of the Ir_2Si plane, is also accompanied by twisting of the Ir_2P_4 core and a concomitant twisting of the silylene group in order to allow the silylene phenyl substituents to occupy the least sterically hindered positions. An alternate mechanism that cannot be ruled out would involve the same types of motions of the diphosphine and silylene bridges, but with the hydride ligands exchanging *between* the metal centers via an intermediate containing two μ-H groups. This would be supported by the slight downfield shift of the hydride resonance (from δ −12.29 to −11.99) upon warming of **4** from −60 °C to room temperature. In previous studies we have found that resonances for bridging hydrides occur downfield of those for terminal hydrides when both types are contained in the same complex,[6,11] so a mechanism in which rapid hydride exchange occurs via a hydride-bridged intermediate should display a downfield shift for this resonance. In contrast, the hydride resonance for complex **2** remains in essentially the same position over a broad range of temperature (δ −11.49 at 23 °C, δ −11.56 at −60 °C), supporting the mechanism proposed in which both hydrides remain terminal throughout the fluxional process. It would appear that like species **2** and **3**, but unlike **5**, the symmetry of the silylene bridge of **4** means that both limiting conformations shown above are energetically equivalent.

The mechanisms proposed for the room-temperature fluxionality of **2**, **3**, and **4** differ from that proposed in the case of $[Rh_2(H)_2(CO)_2(\mu\text{-SiHR})(dppm)_2]$ (R = Et, Ph),[10] where reversible Si–H/Rh–H exchange is believed responsible. For the rhodium dimers, variable-temperature ^1H NMR spectra reveal a scrambling between the rhodium hydrides and the silylene proton under ambient conditions. In our compounds the very slight chemical shift difference for the hydride resonances at ambient and low temperatures is not consistent with a mechanism that involves migration of the hydride from the metal to the silyl moiety during the interchange process. Nor is any resonance observed in compounds **2**, **3**, and **4** for a Si–H unit. In contrast, an SiHPh-bridged dirhodium analogue displayed a hydride signal at ca. δ −4.1 at room temperature that was resolved into two resonances at ca. δ −9.2 and 6.3 in a 2:1 intensity ratio at low temperature.[10] Furthermore, if the fluxionality of the diiridium μ-SiR_2 complexes were similar to that for their dirhodium analogues, the coordinatively

(32) Verkade, J. G.; Quin, L. D., Eds. *Phosphorus-31 NMR Spectroscopy in Stereochemical Analysis*; Methods in Stereochemical Analysis 8; VCH Publishers: Deerfield Beach, FL, 1987.

unsaturated Ir(0) center, generated in the reductive elimination of a silicon–hydrogen bond, might be susceptible to oxidative addition by free $PhSiH_3$; in fact, no such reaction is observed (by ^1H and $^{31}P\{^1H\}$ NMR spectroscopy) when $PhSiH_3$ is added to THF-d_8 solutions containing equimolar amounts of **2**, **3**, or **4**, even after the mixtures are stirred for 24 h at room temperature. As mentioned earlier, the iridium analogue of the above dirhodium complexes, species **5**, is not found to be fluxional, and no evidence of exchange between the iridium- and silicon-bound hydrogens is observed.

Information about the mechanism by which primary or secondary silanes undergo oxidative addition to $[Ir_2(CO)_3(dppm)_2]$ can be obtained by monitoring the reaction of **1** with Ph_2SiH_2 at low temperature, where two intermediates can be observed before formation of the ultimate product, **4**. At −30 °C an unsymmetrical species is observed, which we have formulated as $[Ir_2(H)(CO)_3(SiHPh_2)(dppm)_2]$ (**6**), the result of a single Si–H bond addition at one Ir center. This intermediate appears as two multiplets in the $^{31}P\{^1H\}$ NMR spectrum, at δ −13.6 and −26.7, indicating two inequivalent phosphorus environments, and the $^{13}C\{^1H\}$ NMR spectrum shows two equally intense signals at δ 193.1 and 182.8. The question of whether **6** is a di- or tricarbonyl complex is complicated by the broad carbonyl resonance (at δ 186.7) due to **1**, which is present in at least a 10-fold excess compared to **6** under these conditions and may be obscuring a third resonance due to **6**. In spite of observing only two ^{13}CO resonances, we believe that **6** contains *three* CO ligands, since related studies on the reactions of H_2S and thiols with the mixed-metal dimer $[RhRe(CO)_4(dppm)_2]$, which is isoelectronic with **1**, show that oxidative addition of an S–H bond to the coordinatively unsaturated Rh center takes place to yield the initial products $[RhRe(H)(SR)(CO)_4(dppm)_2]$ (R = H, Et, Ph), with retention of all carbonyl groups, although subsequent CO loss can occur.[8] The ^1H NMR spectrum of **6** shows a triplet in the high-field region at δ −9.40 ($^2J_{P-H}$ = 13.8 Hz), characteristic of a terminal hydride bound to iridium, and also shows a singlet at δ 5.60 of equal intensity, which may be attributed to a proton attached to silicon. Irradiation of only the lower field phosphorus signal leads to collapse of the hydride signal to a singlet. Decoupling of the high-field phosphorus resonance causes no change in these two ^1H signals.

If the sample is warmed to −20 °C, another asymmetric species, **7**, is observed, appearing at δ −6.0 and −7.6 in the phosphorus NMR spectrum. The high-field region of the ^1H spectrum shows, in addition to the resonance at δ −9.40 due to **6**, new triplet signals at δ −3.84 ($^2J_{P-H}$ = 6.8 Hz) and δ −11.86 ($^2J_{P-H}$ = 11.2 Hz). The latter signal appears to be due to a hydride that is terminally bound to iridium, since it collapses to a singlet when the higher field phosphorus signal is decoupled, whereas the lower field hydride signal collapses to a singlet when the lower field phosphorus resonance is irradiated, indicating that it is interacting with a different metal center than the terminal hydride. We propose that the low-field resonance results from a three-centered Ir–H–Si moiety, which may be visualized as an agostic interaction of the Si–H bond with Ir. Such a proposal is supported by the chemical shift value for this hydrogen, which is intermediate between the values expected for a classical hydride and a silicon-bound hydrogen, and also by the low value of $^2J_{P-H}$ relative to typical values observed for terminal iridium hydrides; a three-centered Ir–H–Si interaction would be expected to yield smaller phosphorus–hydrogen coupling values owing to the weaker metal–hydride interaction. In the complexes $[Cp_2Ti(\mu\text{-}H)(\mu\text{-}\eta^2\text{-}HSi(H)Ph)TiCp_2]$[33] and $[(dppm)Mn_2(CO)_6(\mu\text{-}\eta^3\text{-}H_2SiPh_2)]$[34] the ^1H NMR resonances for the agostic M–H–Si units were also found to be intermediate between those for normal Si–H and M–H groups, whereas the signal for the agostic Ir–H–Si interaction in *cis,cis,trans*-$[Ir(PPh_3)_2(\eta^2\text{-}HSiEt_3)_2(H)_2]^+$[35] is actually *upfield* of that for the terminal hydrides and appears to be an exception. Signals due to intermediate **7** in the $^{13}C\{^1H\}$ NMR spectrum could not be unambiguously assigned, since under these conditions significant amounts of species **1**, **4**, and **6**, as well as $[Ir_2(CO)_4(dppm)_2]$[6] (formed by CO addition to **1**), were found to be present in solution. (The absence of the tetracarbonyl species earlier in the reaction, when **6** was the only observed intermediate, is further evidence that carbonyl loss has not occurred in the transformation of **1** to **6**.) Thus, we propose that complex **7** has the formulation $[Ir_2(H)(CO)_2(\mu\text{-}\eta^2\text{-}SiHPh_2)(dppm)_2]$, in which both the terminal hydride ligand and the diphenylsilyl group are attached to the same metal, with an agostic Si–H interaction with the adjacent metal center. Compound **7** can arise readily from species **6** as shown below, via replacement of a carbonyl group by an Si–H interaction. Compound **7** then would represent the immediate precursor to the final product, **4**, via Si–H oxidative addition to Ir. When the sample is warmed to room temperature, **4** is the only species observed in the $^{31}P\{^1H\}$ and ^1H NMR spectra. Compounds **6** and **7** are shown with

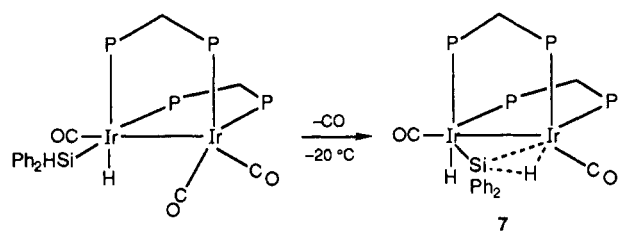

6 **7**

cis diphosphine arrangements, as suggested by the structure determinations of **4** and **5**, as well as that proposed for the precursor **1**.[7] Although the structures for **6** and **7** are not entirely consistent with the hydride resonances observed, which suggest that the hydride ligands are coupled to two equivalent phosphorus nuclei in each compound, it is likely that these intermediates, like the final product (**4**), are fluxional.

Attempts to prepare adducts modeling the first oxidative-addition step were unsuccessful, as the reaction of **1** with Me_3SiH leads to the immediate formation of $[Ir_2(H)_4(CO)_2(dppm)_2]$.[11] It is likely that this reaction proceeds via initial Si–H bond addition at Ir, with subsequent β-hydride elimination from the trimethylsilyl fragment; although β-hydride elimination from a metal–silyl fragment is rare, it has recently been reported for related mononuclear systems.[28,36] The first hydrogenated product so formed would then be $[Ir_2(CO)_2(\mu\text{-}H)_2(dppm)_2]$,[11] which has been shown to react with Me_3SiH to yield the same ultimate product, conceivably through formation of a diiridium trimethylsilyl trihydride that would again undergo β-hydride elimination to give the final tetrahydride. The reaction of Et_3SiH with **1** was also attempted but did not proceed, even under reflux in THF.

(33) Aitken, C. T.; Harrod, J. F., Samuel, E. *J. Am. Chem. Soc.* **1986**, *108*, 4059.
(34) Carreño, R.; Riera, V.; Ruiz, M. A.; Jeannin, Y.; Philoche-Levisalles, M. *J. Chem. Soc., Chem. Commun.* **1990**, 15.
(35) Luo, X.-L.; Crabtree, R. H. *J. Am. Chem. Soc.* **1989**, *111*, 2527.
(36) Berry, D. H.; Procopio, L. J. *J. Am. Chem. Soc.* **1989**, *111*, 4099.

Conclusions

The silylene-bridged dihydride complexes $[Ir_2(H)_2(CO)_2(\mu\text{-}SiRR')(dppm)_2]$ (R = R′ = Me (**2**), Et (**3**), Ph (**4**); R = Ph, R′ = H (**5**)) are readily obtained as the final products of the binuclear oxidative additions of two Si–H bonds of the appropriate silanes to $[Ir_2(CO)_3(dppm)_2]$ (**1**). These stable products cannot be induced to lose H_2 or to react with CO or additional silanes and so are much less labile than their dirhodium analogues, which do react further.[10] Although these iridium species (with the exception of **5**) are fluxional, this fluxionality differs substantially from that displayed by the dirhodium complexes in that hydride exchange between the metal and silicon atoms does not occur. These differences appear to reflect, in part, the greater strength of iridium–hydrogen vs rhodium–hydrogen bonds. The route by which these bridging silylene complexes are formed appears to involve a stepwise process, starting with attack of one Si–H bond of the silane substrate upon the coordinatively unsaturated d^8 Ir(I) center of $[Ir_2(CO)_3(dppm)_2]$ ($[(OC)Ir^+(\mu\text{-}dppm)_2Ir^-(CO)_2]$, as an alternate formulation), followed by loss of CO from, and coordination of the second silicon–hydrogen bond to, the second iridium center, as a prelude to the second oxidative addition and formation of the final silylene-bridged product. Studies of the mechanisms and products of reactions of low-valent binuclear Ir and Rh complexes with other "H_2X"-type substrates are presently underway in this group.

Acknowledgment. We wish to thank the University of Alberta and the Natural Sciences and Engineering Research Council of Canada for support of this work and the NSERC for partial support (through a grant to M.C.) of the diffractometer and structure determination package and for funding of the PE 883 infrared spectrometer. We also thank Prof. R. Eisenberg for a prepublication draft of ref 10b, Prof. U. Schubert for a copy of ref 25 prior to publication, and Dr. R. W. Hilts for advice on NMR simulations.

Supplementary Material Available: Tables of thermal parameters for the anisotropic atoms, idealized hydrogen parameters, and bond distances and angles within the phenyl rings and solvent molecules, along with a summary of crystal data and details of intensity collection for **4** and **5** (13 pages); listings of observed and calculated structure amplitudes for **4** and **5** (39 pages). Ordering information is given on any current masthead page.

Regioselectivity and Stereospecificity in (Trimethylsilyl)methyl Anion Additions to the Functionalized Tungstenocene Derivatives $[W(\eta\text{-}C_5H_4CH_2CR{=}CH_2)(\eta\text{-}C_5H_5)Cl_2]$ (R = H, CH_3)

Thomas C. Forschner, Joseph A. Corella II, and N. John Cooper*

Department of Chemistry, University of Pittsburgh, Pittsburgh, Pennsylvania 15260

Received December 27, 1989

Addition of trimethylsilylmethyllithium to the allyl-substituted tungstenocene dihalides $[W(\eta\text{-}C_5H_4CH_2CR{=}CH_2)(\eta\text{-}C_5H_5)Cl_2]$ (R = H, **1**; R = CH_3, **2**) results in alkylation at the metal center to give $[W(\eta\text{-}C_5H_4CH_2CH{=}CH_2)(\eta\text{-}C_5H_5)\{CH_2Si(CH_3)_3\}_2]$ (**6**) and $[W\{\eta\text{-}C_5H_4CH_2C(CH_3){=}CH_2\}(\eta\text{-}C_5H_5)\{CH_2Si(CH_3)_3\}_2]$ (**8**), respectively. If $(CH_3)_3SiCH_2MgCl$ is used as the carbanion source, the reaction pathways are more complex: with fresh Grignard **2** is still alkylated at the metal to give **8**, but carbomagnesiation of the free double bond of **1** results in formation of a single diastereomer of the unusual carbocyclic $[W\{\eta\text{-}C_5H_4CH_2CH_2CHCH_2Si(CH_3)_3\}(\eta\text{-}C_5H_5)Cl]$ (**4**). Addition of $MgCl_2$ to the Grignard reaction switches the locus of reactivity within **2** and results in alkylation of the cyclopentadienyl ring to form $[W\{\eta\text{-}C_5H_4CH_2Si(CH_3)_3\}\{\eta\text{-}C_5H_4CH_2C(CH_3){=}CH_2\}HCl]$ (**9**).

Introduction

One of the most important current challenges within organotransition-metal chemistry is the development of an understanding, comparable to that which exists in organic chemistry, of the factors controlling the reactivity of organometallic complexes. Our recent discovery[1] that magnesium halides promote the addition of Grignard reagents to the cyclopentadienyl ligands of $[W(\eta\text{-}C_5H_5)_2Cl_2]$ provides access to tungstenocene derivatives with functionalized cyclopentadienyl ligands and has provided us with an interesting opportunity to explore the reactivity of organometallic molecules that offer a number of potentially reactive sites. We have been particularly interested in the allyl-substituted complexes $[W(\eta\text{-}C_5H_4CH_2CH{=}CH_2)(\eta\text{-}C_5H_5)Cl_2]$ (**1**) and $[W\{\eta\text{-}C_5H_4CH_2C(CH_3){=}CH_2\}(\eta\text{-}C_5H_4)Cl_2]$ (**2**), both of which can be prepared conveniently on a multigram scale from $[W(\eta\text{-}C_5H_5)_2Cl_2]$ (**3**)[1]; see eq 1.

Scheme I. Potential Electrophilic Zones of Reactivity within Allyl-Substituted Tungstenocene Dichlorides

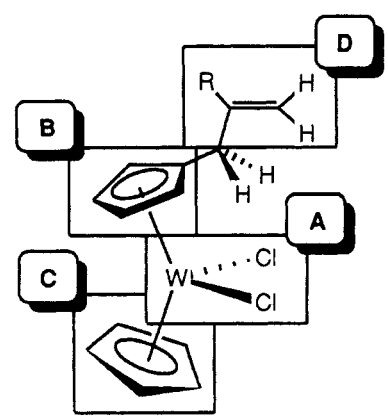

(1) Forschner, T. C.; Cooper, N. J. *J. Am. Chem. Soc.* **1989**, *111*, 7420–7424.

0276-7333/90/2309-2478$02.50/0